Adsorption of tetracycline and sulfonamide antibiotics on amorphous nano-carbon

Yixiao Wu[a], Beidou Xi[b], Guangji Hu[c], Dihua Wang[a], Aimin Li[d], Weihao Zhang[a,e,*], Lei Lu[a], Huijun Ding[a]

[a]School of Resource and Environment Science, Wuhan University, Wuhan 430079, PR China, Tel. +86 27 68777060;
email: zhangwh@whu.edu.cn (W. Zhang)
[b]State Key Lab Environment Criteria & Risk Assessment, Chinese Research Academy of Environmental Sciences,
Beijing 100012, PR China
[c]Environmental Engineering Program, University of Nortdhern British Columbia, Prince George, British Columbia V2N 4Z9,
Canada
[d]Hubei Environmental Monitoring Central Station, Wuhan 430072, PR China
[e]Hubei Provincail Collaborative Innovation Center for Water Resources Security, Wuhan University, Wuhan 430072, PR China

ABSTRACT

Antibiotics in the aquatic environment present potential risks to aquatic ecosystems. The adsorption of tetracycline (TC) and two sulfonamides (SAs), sulfadiazine (SD) and sulfamethoxazole (SMZ), from an aqueous solution of synthesized amorphous nano-carbon (ANC) was investigated. The ANC had a large adsorption capacity for TC (125.55 mg/g), SD (620.74 mg/g), and SMZ (332.21 mg/g). Several mechanisms (i.e. cation exchange, electrostatic interaction, hydrophobic effect, H-bonding, and π–π interactions) are potentially involved in the adsorption process. SAs were more strongly adsorbed on ANC because their molecules are smaller than those of TC. Adsorption nearly reached equilibrium within 2 h, with a removal rate of over 75%. Temperature and pH of the solution positively affected the adsorption process. Cations (Na^+ and Ca^{2+}) in solution had a slight effect on adsorption; Ca^{2+} inhibited adsorption, while Na^+ promoted it. The adsorption process was fitted to pseudo-second-order kinetic and Freundlich models, which indicated that adsorption was both favorable and spontaneous. Fourier transform infrared spectroscopy revealed the interactions between antibiotics and ANC.

Keywords: Nanomaterials; Amorphous carbon; Tetracycline; Sulfonamide; Adsorption

1 Introduction

Several antibiotics, including tetracyclines (TCs) and sulfonamides (SAs), are widely used in the treatment of human and animal diseases, and have been utilized for several decades as food additives to promote animal growth [1]. After taking antibiotics, a large portion is excreted without being metabolized [2]. Because most antibiotics are water-soluble and difficult to degrade, excessive use of such compounds can have severe environmental consequences. For example, some residual antibiotics exert direct toxic effects on environmental micro-organisms [3,4].

*Corresponding author.

They also accelerate the emergence and proliferation of antibiotic-resistant bacteria, thus altering the structure of microbial communities [5]. Some common broad-spectrum antibiotics, such as TCs and SAs, have been frequently detected in ground and surface water [6,7], potential contamination sources for aquatic ecosystems. Therefore, the effective removal of antibiotics from water has recently received much attention.

Inspired by increasing environmental concerns, many treatments have been developed for the removal of antibiotics from water, including ion exchange [8], membrane filtration [9], oxidation [10], and adsorption [11]. Because adsorption can remove target contaminants without producing any noxious byproducts, it has been widely used in practical applications [12]. For example, Yu et al. [13] used oxidized multi-walled carbon nanotubes with different surface oxygen contents as an adsorbent for TCs from aqueous solutions. Blasioli et al. [14] evaluated the removal of sulfamethoxazole (SMZ) by zeolites with high silica content, and found it both effective and irreversible. Among the various adsorbents available, carbon nanomaterials represent ideal candidates for the adsorption of antibiotics due to their high reactivity [15]. They also have a large surface area, rich pore structure, and contain surface functional groups that are beneficial to adsorption. The adsorption of antibiotics by several carbon nanomaterials has been investigated, including graphene oxide [16], carbon nanotubes [17], and magnetic nanocomposites (i.e. Fe_3O_4 coated with carbon) [18]. Antibiotics are believed to be adsorbed on carbon nanomaterials via a hydrophobic effect, π–π interactions, electrostatic interactions, and hydrogen (H)-bonding [19]. Zhang et al. [20] reported that electrostatic and hydrophobic interactions may greatly control the adsorption of SMZ on carbon nanotubes. Gao et al. [11] inferred that the π–π stacking interaction between TC and graphene oxide may serve as the dominant driving force for adsorption.

Yin et al. recently synthesized an amorphous nano-carbon (ANC) with a high removal rate for Cr(VI) [21]. This ANC has a mean pore diameter of 1.54 nm and a large Brunauer–Emmett–Teller (BET) surface area of 616 m^2/g, and contains functional groups on its surface. This ANC has the potential to absorb antibiotics. However, few studies have been conducted on the adsorption capacities of antibiotics. In this work, ANC was used as an adsorbent to absorb TC and two SA antibiotics, sulfadiazine (SD), and SMZ. The adsorption mechanism was evaluated by fitting a kinetic model and considering the adsorption isotherms and thermodynamics. The effects of solution pH and ionic strength on the adsorption process were also investigated.

2. Experimental

2.1. Materials

TC (purity ≥98%, HPLC grade) was purchased from Solarbio Co. (Beijing, China). SD and SMZ (purity ≥98%, HPLC grade) were purchased from Fluka (St. Louis, MO, USA). All other chemicals used were of HPLC grade. The water used in all experiments had a resistivity ≥18 MΩ cm. Properties of the three antibiotics, including chemical structure, molecular weight, log K_{ow}, and pK_a are shown in Table 1.

2.2. Characterization

The ANC was characterized by X-ray diffraction spectroscopy (XRD), scanning electron microscopy, transmission electron microscopy (TEM), confocal Raman microspectroscopy, X-ray fluorescence spectrometry (XRF), and BET analysis. The specific parameters and images are reported elsewhere [21]. The zero-point-of-charge (pH$_{pzc}$) was measured using a Zetasizer (ZEN3600, Malvern Instruments, Malvern, UK). Fourier transform infrared spectroscopy (FTIR) (model 5700, Nicolet, Waltham, MA, USA) was used to identify the species of functional groups. The pore size distribution of the ANC was determined by N_2 adsorption/desorption isotherms using a Quadrasob instrument (SI, Quantachrome, USA).
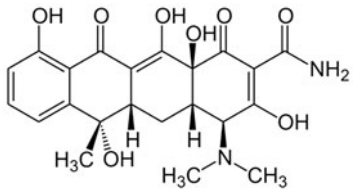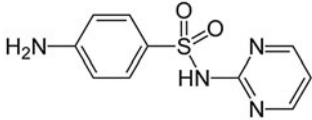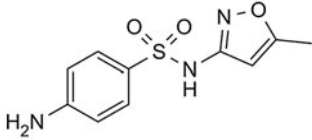
2.3. Adsorption

Batch experiments were conducted to study the adsorption of TC, SD, and SMZ, on ANC from solution. Glass flasks (100 mL) were shaken in a water bath at 25℃ and 160 r/min. Preliminary experiments indicated that adsorption of the antibiotics would reach equilibrium within 17 h. Adsorption capacities of TC, SD, and SMZ on the carbon would reach a maximum at an initial pH of 4, 3, and 3, respectively.

2.3.1. Effect of pH, ionic strength, and temperature on adsorption

The adsorption of TC, SD, and SMZ (6 mg/L) by ANC from solution was measured at pH values ranging from 2 to 11, adjusted using 0.01 mol/L HCl or NaOH. To measure the effects of ionic strength (Ca^{2+} or Na^+) on adsorption, the final $CaCl_2$ and NaCl concentrations were varied from 0 to 0.5 mol/L in acid

Table 1
Physico-chemical properties of TC, SD, and SMZ

Structure	Molecular weight (g/mol)	Molecular volume[a] (cm^3/mol)	log K_{ow}	pK_{a1}	pK_{a2}	pK_{a3}
TC	444.43	270.3 ± 5.0	−1.19 [22]	3.3	7.7	9.7
SD	250.28	167.3 ± 3.0	−0.09 [23]	1.6	6.4	NA
SMZ	253.28	173.1 ± 3.0	0.89[19]	1.7	5.7	NA

[a]Molecular volume of three antibiotics was calculated by ACD/I-Lab.
Note: The ANC was provided by Yin et al. [21].

(pH 4, 3, 3 for TC, SD and SMZ) and neutral (pH 8) solutions, respectively. Temperature was adjusted to 298, 303, 308, and 313 K to investigate the effects of temperature.

2.3.2. Adsorption kinetic and isotherm

For kinetic analysis, 2 mg ANC was added to 50 mL of TC, SD, and SMZ (6 mg/L) solutions at 25℃. Initial pH was then adjusted to 4, 3, and 3, respectively. Samples were taken at different time intervals. To determine adsorption isotherms, 2 mg ANC was placed in 50 mL of TC, SD, and SMZ solutions at different initial concentrations (0–130 mg/L). Residual antibiotics were measured after 17 h in reaction.

The amount of antibiotic adsorption by ANC (q_e, mg/g) was calculated by Eq. (1):

$$q_e = (C_0 - C_t)V/W \qquad (1)$$

where C_0 (mg/L) is the initial concentration of antibiotics, C_t (mg/L) is the concentration of residual antibiotics in solutions after equilibrium, V (L) is the solution volume, and W (g) is the mass of ANC.

2.3.3. Desorption

The solution was immediately filtered through a 0.45-μm filter after equilibrium. ANC was rinsed into 100-mL flasks from the membranes with deionized water. Certain amount of deionized water, $CaCl_2$ or NaCl (0.25 mol/L) solution was added to make the total solution volume 50 mL. After 48 h of oscillating, the antibiotic concentration of the solutions was determined.

2.4. Sample analysis

A UPLC-6460 triple quadrupole liquid chromatography/mass spectrometry (LC/MS) system (Agilent, Santa Clara, CA, USA) was used to determine the concentration of antibiotics in solution. Samples were filtered through a 0.45-μm filter membrane prior to analysis. The specific LC/MS measurement conditions and operating parameters are shown in Tables 2 and 3.

3. Results and discussion

3.1. Adsorbent characterization

Raman spectra results showed a clear characteristic peak of ANC, including a G peak due to the stretching of sp^2 atom pairs in the carboatomic ring or carbochain, and a D peak produced by defects or disorder in materials. XRD spectra also showed that the ANC was amorphous. As with other amorphous carbon materials with similar structures, such as graphene or carbon nanotubes, it can be presumed that

Table 2
Conditions for antibiotics analysis in LC and MS

	Mobile phase	A	0.2% Formic acid and 2 mM ammonium acetate				
		B	Acetonitrile				
LC conditions	Flow	0.3 mL/min					
	Gradient elution	Time (min)	0	0.9	3	4	5
		A (%)	85	80	30	10	85
		B (%)	15	20	70	90	15
	Column	Agilent Eclipse Plus-C18 (100 mm × 2.1 mm, 1.8 µm)					
	Column temperature	40°C					
MS conditions	Ionization source	ESI					
	Gas temperature	325°C					
	Gas flow	5 L/min					
	Sheath gas temperature	350°C					
	Sheath gas flow	11 L/min					

Table 3
UPLC-MS/MS parameters of three antibiotics

	Precursor ion	Product ion	Fragmentor (V)	Collision energy (eV)
TC	445	410.1	130	15
SD	250.9	155.9	100	10
SMZ	254.1	156	110	12

carbon atoms are combined with an sp^2 hybridized covalent bond, while electrons not participating in hybridization form a π bond. XRF analysis indicated that ANC contained 86.39% carbon and 12.7% oxygen, as well as small amounts of other elements as impurities, which produced the D peak in the Raman spectrum.

The presence of impurities results in a variety of functional groups on the ANC surface, thus improving adsorption properties. As shown in Fig. 9, the peak at $3,415 \text{ cm}^{-1}$ corresponds to a hydroxyl group, and the peak at $1,720 \text{ cm}^{-1}$ represents the characteristic stretching band of C=O [24]. The TEM image indicated that ANC is flocculent, containing a large surface area to fully contact other molecules in solution. Because the ANC zero-point-of-charge (pH_{pzc}) is 2.3, when the pH of the solution is higher than 2.3, the ANC is negatively charged; in contrast, it is positively charged at pH values below 2.3.

The Adsorption and desorption isotherms of N_2 at 77 K on ANC are presented in Fig. 1. The Nonlocal Density Functional Theory (NLDFT) model [25] was used to calculate the pore size distribution of the ANC in Fig. 2. As presented in Fig. 1, ANC shows a type II isotherm according to the IUPAC classifications. Many
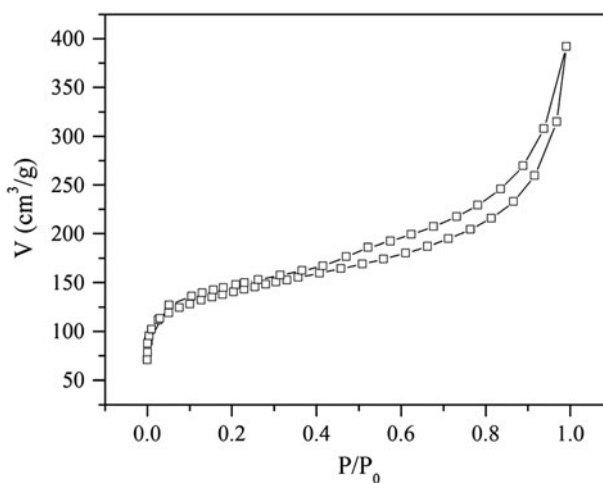

Fig. 1. Adsorption/desorption isotherms of N_2 at 77 K on ANC.

mesoporous and macroporous solids may proceed via multilayer formation in such manner. The amount of adsorbed N_2 increases gradually as the relative pressure increases and the multilayer buildup is abrupt close to the saturation vapor pressure. Besides, the N_2
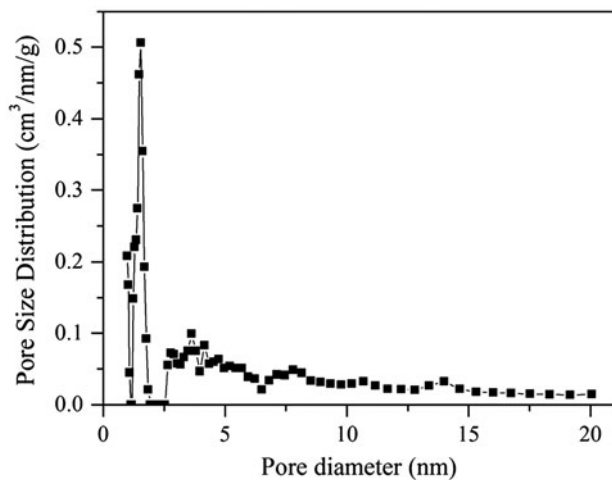
Fig. 2. Pore size distribution of ANC obtained from the NLDFT model of N_2 isotherms.

isotherm on the ANC sample shows a type-H4 hystersis loop attributed to adsorption/desorption in narrow slitlike pores [26]. The total volume of ANC is 0.442 cm^3/g consisted of 37% micropore and 63% mesopore structures. Its mean pore diameter is 1.54 nm.

3.2. Adsorption kinetics

As shown in Fig. 3, the adsorption of antibiotics on ANC was effective. Over 75% of all three antibiotics was removed by the ANC within 2 h, with only a slight increase in adsorption capacity when the duration of treatment was extended beyond 2 h. Adsorption of all three antibiotics reached equilibrium after 17 h of treatment. The highest adsorption capacities of
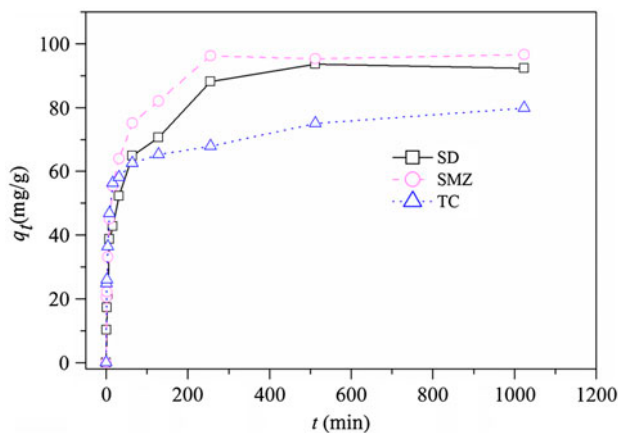

Fig. 3. Effect of adsorption time on adsorption.

TC, SD, and SMZ were 79.8, 92.3, and 96.6%, respectively (i.e. SMZ > SD > TC). The adsorption process is generally considered a competitive adsorption between solvent and adsorbate; therefore, to some extent, the smaller the solubility of the adsorbate, the easier the adsorbate departs from the solvent and is adsorbed on the adsorbent [34]. The log K_{ow} of SMZ was 0.89, the highest of the three antibiotics. As the solubility of SMZ was the lowest, the ANC had a better adsorption performance.

To illustrate the adsorption process, the experimental results were fitted to pseudo-first-order (Eq. (2)) and pseudo-second-order kinetic models (Eq. (3)), and to an intra-particle diffusion model (Eq. (4)):

$$\ln(q_e - q_t) = \ln q_e - k_1 t \tag{2}$$

$$\frac{t}{q_t} = \frac{1}{k_2 q_e^2} + \frac{t}{q_e} \tag{3}$$

$$q_t = k_i t^{0.5} + X \tag{4}$$

Here k_1 (h^{-1}), k_2 (g mg^{-1} h^{-1}), and k_i (g mg^{-1} $h^{-0.5}$) equal the rate constants of pseudo-first-order kinetic, pseudo-second-order kinetic, and intra-particle diffusion models, respectively, where q_t (mg/g) represents the adsorption quantity at t time and X represents the intercept reflecting the boundary layer thickness. The pseudo-first-order kinetic model describes the adsorption of single factors associated with adsorption quantity, while the pseudo-second-order kinetic model describes multiple factors. The intra-particle diffusion model was used to determine the rate-limiting process.

Table 4 shows R^2 values, and indicates that the pseudo-second-order kinetic model is more suitable for describing the adsorption processes of the three antibiotics. The pseudo-second-order kinetic model assumes that adsorption rates are controlled by the chemical adsorption mechanism, and therefore describes a chemical adsorption process related to electron transfer or sharing. For TC, k_1 was the lowest of the three antibiotics, whereas k_2 was the highest, suggesting that the physical adsorption process of TC was the slowest and the chemical adsorption process was the fastest. It was also apparent that the data for the first 30 min of adsorption fitted the pseudo-first-order kinetic model well, indicating that the initial adsorption process was controlled by a single factor.

The adsorption process of the three antibiotics on ANC can be divided into three periods. The first is the interaction between antibiotic molecules and active adsorption sites on the ANC. The second is the rapid intra-particle diffusion process, in which adsorption

Table 4
The kinetic parameters of TC, SD, and SMZ adsorption on ANC

	C_0 (mg/L)	$q_{e,exp}$ (mg/g)	Pseudo-first-order model			Pseudo-second-order model		
			$k_1 \times 10^{-2}$	$q_{e,cal}$ (mg/g)	R^2	$k_2 \times 10^{-2}$	$q_{e,cal}$ (mg/g)	R^2
TC	6	79.85	0.44	37.96	0.7228	0.092	79.55	0.9976
SD	6	93.55	0.83	65.95	0.9643	0.057	94.34	0.9986
SMZ	6	96.66	1.07	57.96	0.9280	0.087	97.94	0.9995

occurs in the micropores of the ANC. The final period is a slow intra-particle diffusion process with an increase in the boundary layer effect. The three periods of adsorption can be seen in Fig. 4(c). The rate constant, k_i, and intercept, X, were calculated for each of the three periods (Table 5). There were no significant differences in k_i in the first and last periods for all three antibiotics, whereas k_i was larger for SD and SMZ than for TC, indicating that the water film resistance caused by SD and SMZ surrounding ANC particles may be weaker than that caused by TC. Therefore, SD and SMZ can be transported more easily from the liquid film layer to the external surface of the ANC [35].
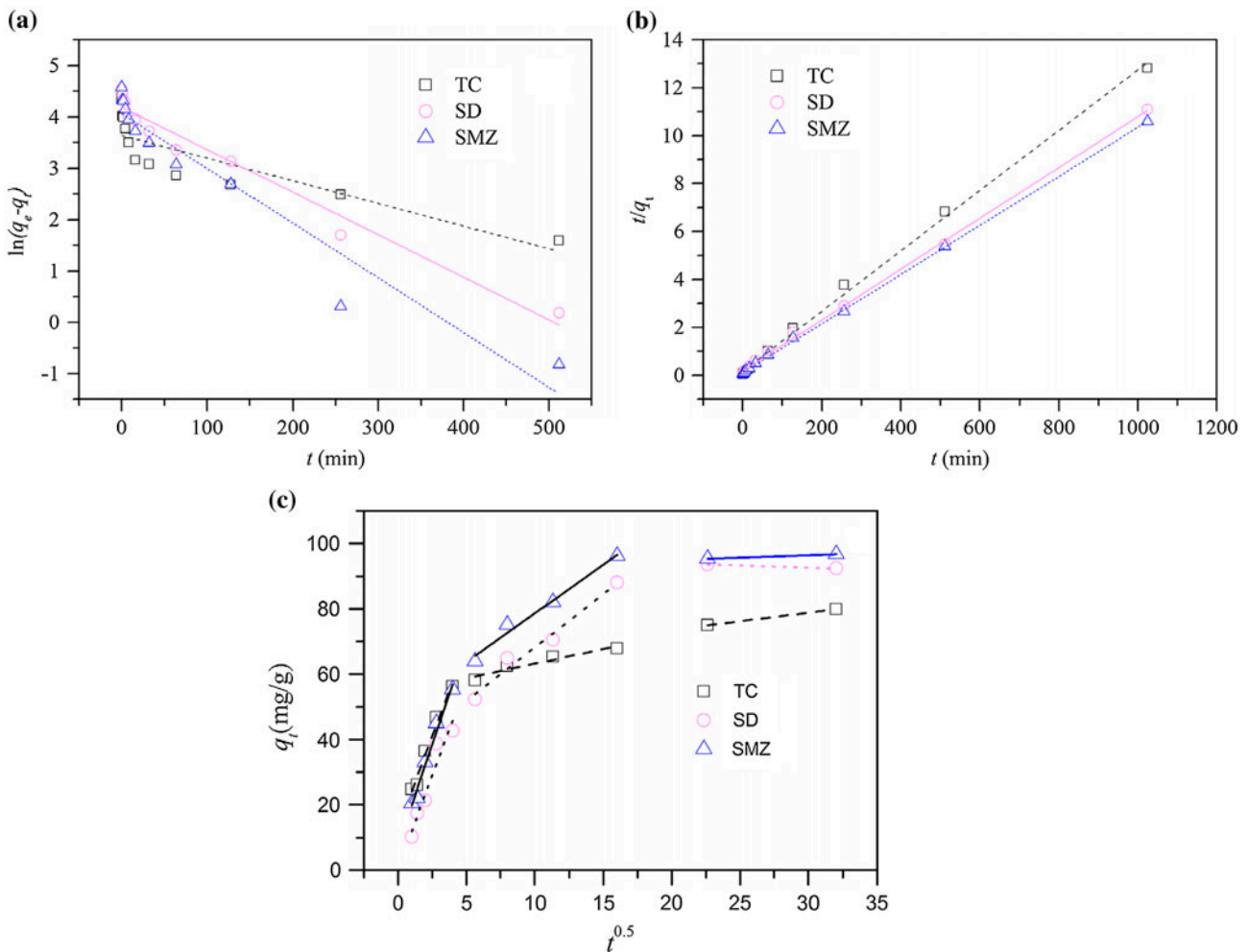

Fig. 4. The pseudo-first-order kinetics model (a), pseudo-second-order kinetics model (b) and the intra-particle diffusion model (c) of adsorption process.

Table 5
Intra-particle diffusion model parameters of TC, SD, and SMZ adsorption on ANC

	Adsorption process	k_i (g mg^{-1} h$^{-0.5}$)	X	R^2
TC	1	11.18	12.89	0.9892
	2	0.89	54.28	0.9623
	3	0.52	63.12	0.9999
SD	1	11.31	0.61	0.9653
	2	3.27	35.41	0.9871
	3	−0.13	96.46	0.9999
SMZ	1	12.36	7.42	0.9896
	2	2.99	48.73	0.9910
	3	0.14	92.04	0.9999

3.3. Effects of initial pH values and coexisting cations

Solution pH values can affect both surface charge and density of the ANC, as well as degree of protonation of the three antibiotics. Because polar and ionizable functional groups are present in TC and SA molecules, these molecules can be ionized into cationic species when pH < pK_{a1}. The ANC surface is overall negatively charged at pH > 2.3 (pH$_{pzc}$). Therefore, cationic antibiotic molecules can combine with the ANC via cation exchange and electrostatic interaction when the pH is close to pH$_{pzc}$. As shown in Fig. 5, the highest adsorption capacities of TC, SD, and SMZ on ANC were observed when the initial pH was 4, 3, and 3, respectively. All three antibiotic molecules contain benzene rings and an aromatic heterocyclic group, and have strong electron withdrawal abilities and specific π-electron acceptor properties. Therefore,
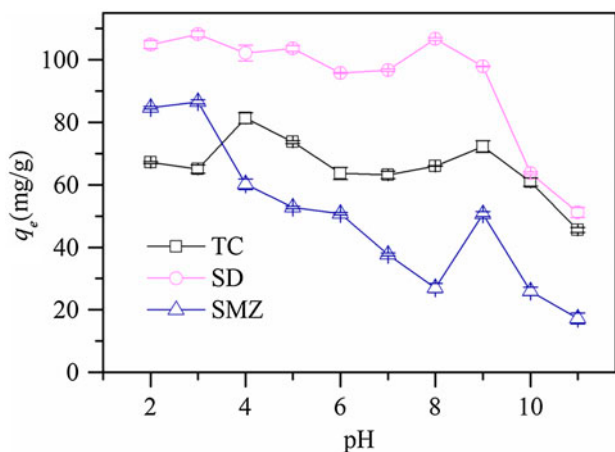
antibiotic molecules can combine on ANC by π–π electron donor–acceptor interactions [19]. Moreover, they can also be combined by the action of H-bonds, due to the functional groups containing oxygen on the antibiotic molecules and ANC surface.

However, adsorption capacities of the three antibiotics decreased as the initial pH increased (higher than 4, 3, and 3, respectively). This was due to the dominance of the zwitterion when the pH was between pK_{a1} and pK_{a2}, which may weaken the interaction between the antibiotics and ANC by electrostatic repulsion [27].

When pH > pK_{a2}, anionic species are dominant in solution. Adsorption capacities of the three antibiotics clearly enhanced electrostatic repulsion. As shown in Fig. 5, the ANC was also able to adsorb antibiotic anions in weak basic solutions (pH 8 and 9). Therefore, non-electrostatic interactions, such as cation bridging, could be attributed to adsorption at high pH [28,29].

The influence of different Ca^{2+} and Na$^+$ concentrations on adsorption in solution with different initial pH values is shown in Fig. 6(a) and (b). At pH 8, the effects of Ca^{2+} and Na$^+$ are more obvious especially for TC. TC and SMZ adsorptions with NaCl increase with the ionic concentration, which may be contributed to salting out effect. When NaCl is added, the solubility of TC and SMZ is decreased, facilitating the diffusion of more antibiotics to the surface of ANC, resulting in increased adsorption [23]. As the anionic forms are the main species in the aqueous solutions at pH 8, while the cationic and neutral forms are dominant in acid solutions, the effects of Na$^+$ are expected to be stronger on anionic species because of the strong electrostatic interactions [19]. Of the three antibiotics, Ca^{2+} had the strongest inhibition effect on TC adsorption. The chelation reactions can occur between TC molecules and metal cations [30], which may enlarge the molecular size of Ca^{2+}–TC complex resulting in less adsorption capacity of TC molecules for ANC [31].

When solutions are acid (pH 4, 3, and 3 for TC, SD, and SMZ, respectively), Na$^+$ and Ca^{2+} had no significant effect on adsorption; however, Ca^{2+} resulted in a slight inhibition, while Na$^+$ had the opposite effect. During adsorption, Ca^{2+} may compete with cationic TC molecules for adsorption on ANC. Other researchers have suggested that the presence of electrolyte solutions may change the strength of the interaction between antibiotics and carbon due to electrostatic shielding effects [32]. With respect to Na$^+$, the slight increase in adsorption may be due to cation bridging between the ANC and antibiotic molecules [33]. The different trends of acid and weak alkaline
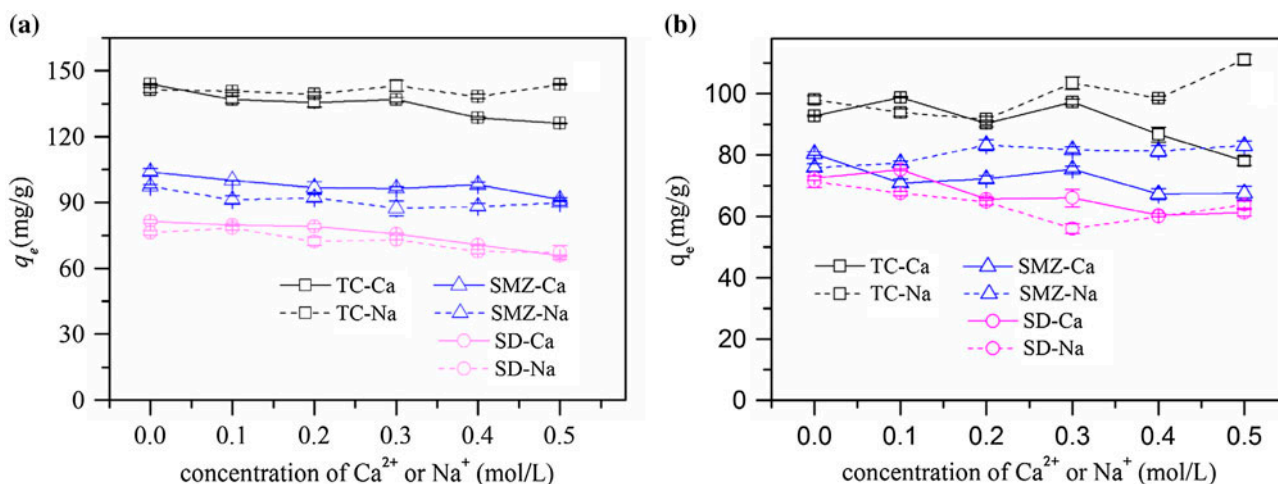

Fig. 5. Effects of the initial pH on adsorption.

Fig. 6. Effects of coexisting cations (Ca^{2+} and Na^+) in acid (a) and weak alkaline solutions on adsorption.

solutions may be due to the complex adsorption mechanisms.

3.4. Adsorption isotherms

Adsorption isotherm data were fitted to the Freundlich (Eq. (5)) and Langmuir (Eq. (6)) isotherm models:

$$q_e = K_F C_e^{1/n} \tag{5}$$

$$q_e = \frac{Q_m K_L C_e}{1 + K_L C_e} \tag{6}$$

where K_F ($mg^{1-1/n} \, L^{1/n} \, g^{-1}$) represents the Freundlich constant, which is related to adsorption capacity, K_L (L/mg) represents the Langmuir adsorption equilibrium constant, which is related to adsorption energy and the affinity of adsorbate to adsorbent, n represents the constant of adsorption strength, and Q_m (mg/g) represents maximum adsorption capacity.

The Langmuir isotherm assumes that the adsorption sites are distributed uniformly on the entire surface of the adsorbent, with adsorbate molecules only adsorbed on specific sites and each site accepting only one particle. However, in reality, there are often several sites on the adsorbent surface with different adsorption energies. Unlike the Langmuir isotherm, the Freundlich isotherm assumes that adsorption occurs on a non-uniform surface. As shown in Fig. 7 and Table 6, with the exception of SMZ, the adsorption fitted the Freundlich isotherm model better, as identified by the determination coefficient, R^2. The

parameter $1/n$ of the Freundlich model indicates if adsorption is linear. The $1/n$ values of the three adsorption processes were 0.22, 0.39, and 0.20, respectively, indicating that all adsorption processes were non-linear and effective [29]. The values were all less than 1, indicating the presence of more heterogeneous adsorption sites on the ANC due to particular adsorption interactions [13,36].

Maximum adsorption capacities of the three antibiotics were calculated by the Langmuir isotherm, and indicated good adsorption properties of the carbon compared to other adsorbents (Table 7). As shown in Table 6, the ANC was selective in its adsorption of the three antibiotics, with q_m of the three antibiotics being 125.55, 620.74, and 332.21 mg/g, respectively; this may be associated with the pore structure inside the ANC. Adsorbate molecules always have orientation and sieving effects during adsorption. When the size of adsorbate molecules is close to the pore size, adsorption is strong. In contrast, when the size of the adsorbate molecule is larger than the pore size, it is difficult for the molecules to enter the adsorbent pores [23]. Micropores (<2 nm) are commonly found in carbons, but larger TC molecules cannot easily enter. Ji et al. [37] also proved that carbon nanotubes better adsorbed small SA molecules.

3.5. Adsorption thermodynamics

To determine the effect of temperature, adsorption was investigated at temperatures ranging from 298 to 313 K. The thermodynamic equations used are shown below:
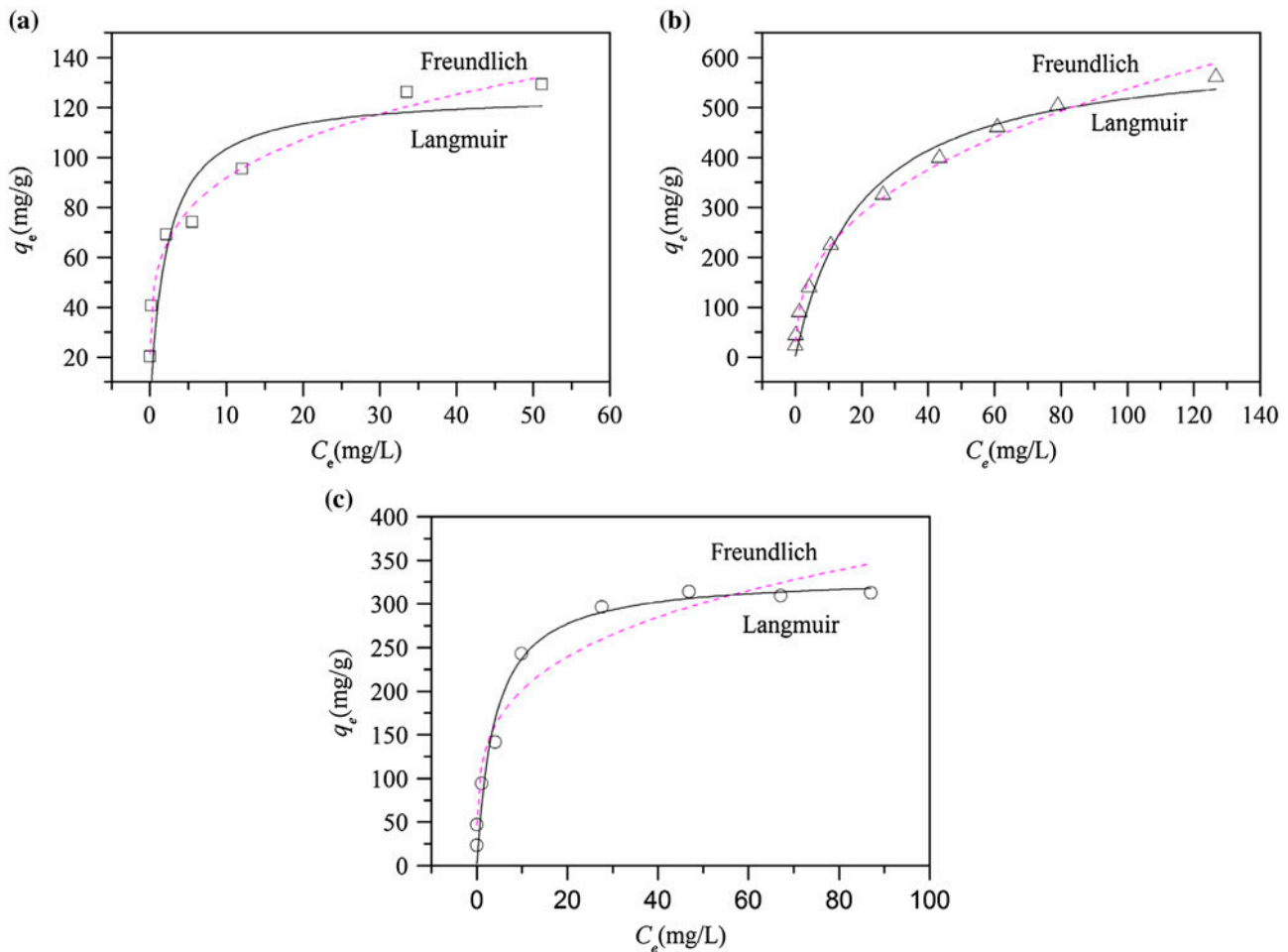
Fig. 7. The Freundlich and Langmuir isotherms of TC (a), SD (b), and SMZ (c) adsorption processes.

Table 6
The isotherm parameters of TC, SD, and SMZ adsorption on ANC

		Freundlich			Langmuir		
	T	K_F	$1/n$	R^2	K_L	q_m (mg/g)	R^2
TC	298	56.98	0.22	0.9877	0.47	125.55	0.7846
SD	298	89.21	0.39	0.9943	0.05	620.74	0.9636
SMZ	298	113.19	0.20	0.9401	0.25	332.21	0.9754

$$K_d = \frac{q_e}{C_e} \tag{7}$$

$$\ln K_d = \frac{-\Delta H^\circ}{RT} + \frac{\Delta S^\circ}{R} \tag{8}$$

$$\Delta G^\circ = \Delta H^\circ - T\Delta S^\circ \tag{9}$$

where K_d represents the partition coefficient, ΔH° (kJ/mol) represents enthalpy change, ΔS° (J mol^{-1} K^{-1}) represents entropy change, ΔG° (kJ/mol) represents the change in Gibbs free energy, T (K) represents thermodynamic temperature, and R represents the gas constant (8.314 J mol^{-1} K^{-1}). ΔH° and ΔS° were obtained from the slope and intercept of the linear plot of $\ln K_d$ vs. $1/T$.

As shown in Table 8, the adsorption capacity increased with increasing temperatures (from 298 to 313 K). The increase in temperature can enhance the rate of molecular diffusion and decrease the viscosity of the solution. Thus, it is easier for sorbate molecules to cross the external boundary layer and move into the internal pores of sorbents [45]. As the ΔH° of the three antibiotics was positive, the adsorption was endothermic. The data also confirmed that the adsorption capacities increased with temperature. Positive ΔS° values indicate increased randomness at the solid/solution interface during adsorption [46]. As the

Table 7
Comparison of maximum adsorption capacity (q_{m}) for antibiotics of different adsorbents

Adsorbent	q_{m} (mg/g)	Specific surface area (m²/g)	Mean pore diameter (nm)	Refs.
For TC				
Oxidized multi-walled carbon nanotubes	269	471	6	[13]
Multi-walled carbon nanotubes	27–38	167–185	5–10	[38]
Magnetic nanocomposite	43	155	7	[39]
Mesoporous silica	43	245	6	[40]
Bio-char	95	128	–	[41]
ANC	125	616	1	This work
For SD				
Magnetic ion-exchange resins	461	7	3	[42]
ANC	620	616	1	This work
For SMZ				
Powdered activated carbon from pine tree	131	453	1	[43]
Carbon nanotube	98	113	–	[44]
Carbon-coated magnetic nanocomposite	126	44	17	[18]
ANC	332	616	1	This work

Table 8
The thermodynamic parameters of adsorption processes

	T (K)	q_{e} (mg/g)	$\Delta G°$ (kJ/mol)	$\Delta H°$ (kJ/mol)	$\Delta S°$ (J mol^{-1} K^{-1})
TC	298	79.85	−14.1917	52.3807	223.3972
	303	97.14	−15.3087		
	308	101.01	−16.4256		
	313	129.54	−17.5426		
SD	298	90.67	−9.0736	34.9429	147.7065
	303	95.31	−9.8122		
	308	103.30	−10.5507		
	313	110.56	−11.2892		
SMZ	298	96.67	−9.5108	33.4330	144.1066
	303	99.31	−10.2313		
	308	109.30	−10.9518		
	313	113.56	−11.6724		

temperature increased, $\Delta G°$ gradually decreased, demonstrating that a higher temperature had a positive effect on adsorption. $\Delta G°$ reflected the adsorption driving force, with negative values indicating spontaneity of adsorption.

3.6. Desorption

The desorption results can be seen in Fig. 8. The desorption rates of the three antibiotics are low in contrast with the adsorption results, as the desorption values were below 30%. It indicates the hysteresis affects the adsorption/desorption processes [47]. This hysteresis is related to the strong bonds established between the antibiotics and the adsorbent surfaces [48]. The low desorption rates by Na$^+$ and Ca^{2+} also demonstrate that cation exchange may be one, but not the, main mechanism. Among the three antibiotics, the desorption efficiencies of SD molecules caused by presence of Ca^{2+} is highest, followed by SMZ.
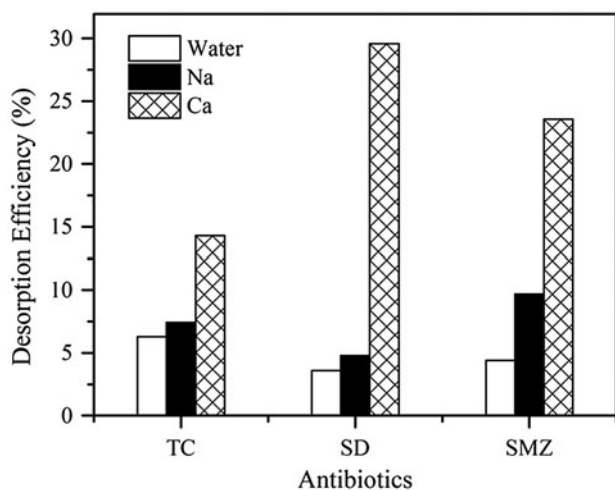
Fig. 8. The desorption efficiency of TC, SD, and SMZ from ANC in solutions with or without Na^+ and Ca^{2+}.
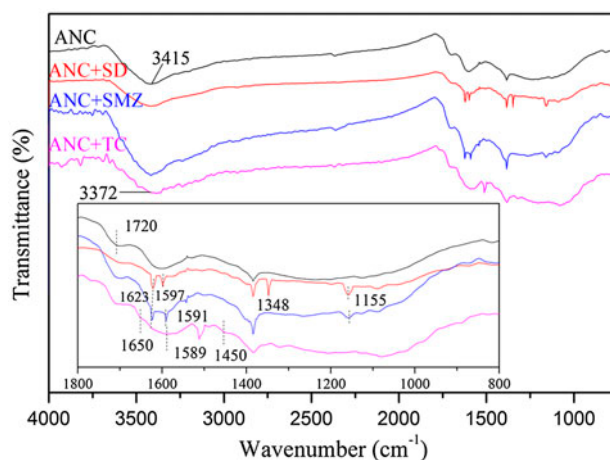

Fig. 9. The FTIR absorption spectra of ANC before and after treatment with 50 mg/L TC, SD, and SMZ solutions. Insert showed the spectra of peaks from 800 to 1800 cm^{-1}.

The differences between SD and SMZ are not obvious, as the molecular size of two antibiotics is close. However, the TC is hard to be desorbed from the carbon, probably due to the bigger molecular size, which is harder to be desorbed from the inner structure of ANC [49].

3.7. FTIR analyses

FTIR was used to confirm interactions between the antibiotics and ANC. Fig. 9 shows the characteristic peaks of the three antibiotics on ANC following adsorption. For TC, the peaks at 1,615, 1,583, and 1,448 cm^{-1} could be assigned to the C=O stretching in the A ring, C=O stretching in the C ring, and stretching in the C=C skeleton, respectively. However, there were slight shifts to higher wavenumbers (i.e. 1,650, 1,589, and 1,450 cm^{-1}), indicating an increased interaction between TC and ANC (Fig. 6) [50]. The hydroxyl peak in the ANC changed, especially following adsorption of TC (from 3,415 to 3,372 cm^{-1}), which may be attributed to H-bonding between the antibiotics and ANC, thus restricting vibration of the hydroxyl moiety [41]. For SD and SMZ, the peak at 1,155 cm^{-1} suggests stretching of the sulphonyl group in SD and SMZ, while the peak at 1,591 cm^{-1} is associated with the isoxazole ring in SMZ [51], demonstrating the adsorption occurred between SA molecules and ANC. At lower frequencies, the peak at 1,614 cm^{-1} is due to the heterocycle ring C-N vibrations of SMZ, which is upshifted to 1,623 cm^{-1} after adsorption onto ANC. This may be consistent with the occurrence of van der Waals interactions between

SMZ heterocycle ring and the ANC [14]. For SD, the peak at 1,623 cm^{-1} assigned to the bending frequency of the amino group, shows an upward shift to 1,629 cm^{-1}, which can be contributed to H-bonding. And the limited changes of benzene at 1,597 and 1,348 cm^{-1} for SD indicate an interaction of aromatic rings with ANC [52].

4. Conclusion

In this study, one type of ANC was selected to test the adsorption of one TC and two SA (SD and SMZ) antibiotics. ANC exhibited good adsorption properties for all three antibiotics, as expected. The adsorption was pH-dependent, and different forms of antibiotic ions combined with ANC via different mechanisms, including cation exchange, electrostatic interaction, hydrophobic effect, H-bonding, and π–π electron donor–acceptor interactions. Maximum adsorption capacities for TC, SD, and SMZ were 125.55, 620.74, and 332.21 mg/g at 298 K, in which the initial pH values were 4, 3, and 3, respectively. The cations in solution had a slight effect on adsorption, with Ca^{2+} inhibiting adsorption and Na^+ promoting it. A pseudo-second-order model fitted the whole adsorption process well, while a pseudo-first-order model was suitable to describe adsorption before 30 min. The adsorption nearly reached equilibrium within 2 h, with a removal rate of over 75%. The intra-particle diffusion model revealed three periods of adsorption. The data fitted the Freundlich isotherm well, indicating that adsorption was non-linear and effective. Calculation of the adsorption thermodynamics revealed

that adsorption was both endothermic and spontaneous. The forces between antibiotic molecules and ANC are strong as the desorption efficiency is low. Small shifts were observed in characteristic peaks from the FTIR adsorption spectra, indicating interactions between the antibiotics and ANC.

Acknowledgments

References

[1] B. Halling-Sorensen, S.N. Nielsen, P.F. Lanzky, F. Ingerslev, H.C.H. Lutzhoft, S.E. Jorgensen, Occurrence, fate and effects of pharmaceutical substances in the environment—A review, Chemosphere 36 (1998) 357–394.

[2] N. Milić, M. Milanović, N.G. Letić, M.T. Sekulić, J. Radonić, I. Mihajlović, M.V. Miloradov, Occurrence of antibiotics as emerging contaminant substances in aquatic environment, Int. J. Environ. Health Res. 23 (2013) 296–310.

[3] W.W. Yang, Z.P. Tang, F.Q. Zhou, W.H. Zhang, L.R. Song, Toxicity studies of tetracycline on *Microcystis aeruginosa* and *Selenastrum capricornutum*, Environ. Toxicol. Pharmacol. 35 (2013) 320–324.

[4] M.D. Hernando, M. Mezcua, A.R. Fernandez-Alba, D. Barcelo, Environmental risk assessment of pharmaceutical residues in wastewater effluents, surface waters and sediments, Talanta 69 (2006) 334–342.

[5] S.J. Harris, M. Cormican, E. Cummins, Antimicrobial residues and antimicrobial-resistant bacteria: impact on the microbial environment and risk to human health— A review, Hum. Ecol. Risk Assess. 18 (2012) 767–809.

[6] Y.M. Wei, Y. Zhang, J. Xu, C.S. Guo, L. Li, W.H. Fan, Simultaneous quantification of several classes of antibiotics in water, sediments, and fish muscles by liquid chromatography-tandem mass spectrometry, Front. Environ. Sci. Eng. 8 (2014) 357–371.

[7] D.M. Cheng, X.H. Liu, L. Wang, W.W. Gong, G.N. Liu, W.J. Fu, M. Cheng, Seasonal variation and sediment–water exchange of antibiotics in a shallower large lake in North China, Sci. Total Environ. 476–477 (2014) 266–275.

[8] A.M.L. Fernández, M. Rendueles, M. Díaz, Sulfamethoxazole removal from synthetic solutions by ion exchange using a strong anionic resin in fixed bed, Solvent Extr. Ion Exch. 31 (2013) 763–781.

[9] J. Radjenović, M. Petrović, D. Barceló, Fate and distribution of pharmaceuticals in wastewater and sewage sludge of the conventional activated sludge (CAS) and advanced membrane bioreactor (MBR) treatment, Water Res. 43 (2009) 831–841.

[10] F.J. Beltrán, A. Aguinaco, J.F. García-Araya, A.L. Oropesa, Ozone and photocatalytic processes to remove the antibiotic sulfamethoxazole from water, Water Res. 42 (2008) 3799–3808.

[11] Y. Gao, Y. Li, L. Zhang, H. Huang, J.J. Hu, S.M. Shah, X.G. Su, Adsorption and removal of tetracycline antibiotics from aqueous solution by graphene oxide, J. Colloid Interface Sci. 368 (2012) 540–546.

[12] V. Homem, L. Santos, Degradation and removal methods of antibiotics from aqueous matrices—A review, J. Environ. Manage. 92 (2011) 2304–2347.

[13] F. Yu, J. Ma, S. Han, Adsorption of tetracycline from aqueous solutions onto multi-walled carbon nanotubes with different oxygen contents, Sci. Rep. 4 (2014) 5326.

[14] S. Blasioli, A. Martucci, G. Paul, L. Gigli, M. Cossi, C.T. Johnston, L. Marchese, I. Braschi, Removal of sulfamethoxazole sulfonamide antibiotic from water by high silica zeolites: A study of the involved host–guest interactions by a combined structural, spectroscopic, and computational approach, J. Colloid Interface Sci. 419 (2014) 148–159.

[15] M.M. Khin, A.S. Nair, V.J. Babu, R. Murugan, S. Ramakrishna, A review on nanomaterials for environmental remediation, Energy Environ. Sci. 5 (2012) 8075–8109.

[16] G.Z. Kyzas, E.A. Deliyanni, K.A. Matis, Graphene oxide and its application as an adsorbent for wastewater treatment, J. Chem. Technol. Biotechnol. 89 (2014) 196–205.

[17] Y. Tian, B. Gao, V.L. Morales, H. Chen, Y. Wang, H. Li, Removal of sulfamethoxazole and sulfapyridine by carbon nanotubes in fixed-bed columns, Chemosphere 90 (2013) 2597–2605.

[18] X.L. Bao, Z.M. Qiang, J.H. Chang, W.W. Ben, J.H. Qu, Synthesis of carbon-coated magnetic nanocomposite (Fe3O4@C) and its application for sulfonamide antibiotics removal from water, J. Environ. Sci. 26 (2014) 962–969.

[19] L.L. Ji, W. Chen, S.R. Zheng, Z.Y. Xu, D.Q. Zhu, Adsorption of sulfonamide antibiotics to multiwalled carbon nanotubes, Langmuir 25 (2009) 11608–11613.

[20] D. Zhang, B. Pan, H. Zhang, P. Ning, B.S. Xing, Contribution of different sulfamethoxazole species to their overall adsorption on functionalized carbon nanotubes, Environ. Sci. Technol. 44 (2010) 3806–3811.

[21] H.Y. Yin, X.H. Mao, D.Y. Tang, W. Xiao, L.R. Xing, H. Zhu, D.H. Wang, D.R. Sadoway, Capture and electrochemical conversion of CO2 to value-added carbon and oxygen by molten salt electrolysis, Energy Environ. Sci. 6 (2013) 1538–1545.

[22] J. Tolls, Sorption of veterinary pharmaceuticals in soils: A review, Environ. Sci. Technol. 35 (2001) 3397–3406.

[23] W.B. Yang, F.F. Zheng, X.X. Xue, Y.P. Lu, Investigation into adsorption mechanisms of sulfonamides onto porous adsorbents, J. Colloid Interface Sci. 362 (2011) 503–509.

[24] T. Ramanathan, F.T. Fisher, R.S. Ruoff, L.C. Brinson, Amino-functionalized carbon nanotubes for binding to polymers and biological systems, Chem. Mat. 17 (2005) 1290–1295.

[25] A.V. Neimark, P.I. Ravikovitch, M. Grün, F. Schüth, K.K. Unger, Pore size analysis of MCM-41 Type adsorbents by means of nitrogen and argon adsorption, J. Colloid Interface Sci. 207 (1998) 159–169.

[26] M. Kruk, M. Jaroniec, Gas adsorption characterization of ordered organic-inorganic nanocomposite materials, Chem. Mat. 13 (2001) 3169–3183.

[27] N. Anderson, A.J. Rubin, Adsorption of Inorganics at Solid-Liquid Interfaces, Ann Arbor Science, Ann Arbor, 1981.

[28] P. Hongsawat, P. Prarat, C. Ngamcharussrivichai, P. Punyapalakul, Adsorption of ciprofloxacin on surface functionalized superparamagnetic porous silicas, Desalin. Water Treat. 52 (2014) 4430–4443.

[29] Y. Ma, Q. Zhou, S.C. Zhou, W. Wang, J. Jin, J.W. Xie, A.M. Li, C.D. Shuang, A bifunctional adsorbent with high surface area and cation exchange property for synergistic removal of tetracycline and Cu^{2+}, Chem. Eng. J. 258 (2014) 26–33.

[30] M. Wan, Z.H. Li, H.L. Hong, Q.F. Wu, Enrofloxacin uptake and retention on different types of clays, J. Asian Earth Sci. 77 (2013) 287–294.

[31] P.H. Chang, Z.H. Li, J.S. Jean, W.T. Jiang, C.J. Wang, K.H. Lin, Adsorption of tetracycline on 2:1 layered non-swelling clay mineral illite, Appl. Clay Sci. 67–68 (2012) 158–163.

[32] M.E. Parolo, M.J. Avena, M.C. Savini, M.T. Baschini, V. Nicotra, Adsorption and circular dichroism of tetracycline on sodium and calcium-montmorillonites, Colloids Surf., A 417 (2013) 57–64.

[33] M.F. Xia, A.M. Li, Z.L. Zhu, Q. Zhou, W.B. Yang, Factors influencing antibiotics adsorption onto engineered adsorbents, J. Environ. Sci. 25 (2013) 1291–1299.

[34] L.R. Radovic, C.M. Castilla, J.R. Utrilla, Carbon materials as adsorbents in aqueous solutions, in: L.R. Radovic, (Ed.), Chemistry and Physics of Carbon, vol. 27, 2001, pp. 227–405.

[35] X.P. Qin, F. Liu, G.C. Wang, L.P. Weng, L. Li, Adsorption of levofloxacin onto goethite: Effects of pH, calcium and phosphate, Colloids Surf., B 116 (2014) 591–596.

[36] H. Kim, Y.S. Hwang, V.K. Sharma, Adsorption of antibiotics and iopromide onto single-walled and multi-walled carbon nanotubes, Chem. Eng. J. 255 (2014) 23–27.

[37] L.L. Ji, Y. Shao, Z.Y. Xu, S.R. Zheng, D.Q. Zhu, Adsorption of monoaromatic compounds and pharmaceutical antibiotics on carbon nanotubes activated by KOH etching, Environ. Sci. Technol. 44 (2010) 6429–6436.

[38] Q.Q. Yang, G.C. Chen, J.F. Zhang, H.L. Li, Adsorption of sulfamethazine by multi-walled carbon nanotubes: Effects of aqueous solution chemistry, RSC Adv. 5 (2015) 25541–25549.

[39] G.A. Akkaya Sayğılı, H. Sayğılı, F. Koyuncu, F. Güzel, Development and physicochemical characterization of a new magnetic nanocomposite as an economic antibiotic remover, Process Saf. Environ. Prot. 94 (2015) 441–451.

[40] Z.Y. Zhang, H.C. Lan, H.J. Liu, J.H. Qu, Removal of tetracycline antibiotics from aqueous solution by amino-Fe (III) functionalized SBA15, Colloids Surf., A 471 (2015) 133–138.

[41] L. Peng, Y.Q. Ren, J.D. Gu, P.F. Qin, Q.R. Zeng, J.H. Shao, M. Lei, L.Y. Chai, Iron improving bio-char derived from microalgae on removal of tetracycline from aqueous system, Environ. Sci. Pollut. Res. 21 (2014) 7631–7640.

[42] M. Jiang, W. Yang, Z. Zhang, Z. Yang, Y. Wang, Adsorption of three pharmaceuticals on two magnetic ion-exchange resins, J. Environ. Sci. (China) 31 (2015) 226–234.

[43] M.C. Tonucci, L.V.A. Gurgel, S.F. Aquino, Activated carbons from agricultural byproducts (pine tree and coconut shell), coal, and carbon nanotubes as adsorbents for removal of sulfamethoxazole from spiked aqueous solutions: Kinetic and thermodynamic studies, Ind. Crop. Prod. 74 (2015) 111–121.

[44] Y. Tian, B. Gao, H. Chen, Y. Wang, H. Li, Interactions between Carbon Nanotubes and Sulfonamide Antibiotics in Aqueous Solutions under Various Physicochemical Conditions, J. Environ. Sci. Health Part A Toxic/ Hazard. Subst. Environ. Eng. 48 (2013) 1136–1144.

[45] Z.Y. Wang, X.D. Yu, B. Pan, B.S. Xing, Norfloxacin sorption and its thermodynamics on surface-modified carbon nanotubes, Environ. Sci. Technol. 44 (2010) 978–984.

[46] S. Jain, R.K. Vyas, P. Pandit, A.K. Dalai, Adsorption of antiviral drug, acyclovir from aqueous solution on powdered activated charcoal: Kinetics, equilibrium, and thermodynamic studies, Desalin. Water Treat. 52 (2014) 4953–4968.

[47] D. Fernandez-Calvino, A. Bermudez-Couso, M. Arias-Estevez, J.C. Novoa-Munoz, M.J. Fernandez-Sanjurjo, E. Alvarez-Rodriguez, A. Nunez-Delgado, Competitive Adsorption/Desorption of Tetracycline, Oxytetracycline and Chlortetracycline on Two Acid Soils: Stirred Flow Chamber Experiments, Chemosphere 134 (2015) 361–366.

[48] D. Fernández-Calviño, A. Bermúdez-Couso, M. Arias-Estévez, J.C. Nóvoa-Muñoz, M.J. Fernández-Sanjurjo, E. Álvarez-Rodríguez, A. Núñez-Delgado, Kinetics of tetracycline, oxytetracycline, and chlortetracycline adsorption and desorption on two acid soils, Environ. Sci. Pollut. Res. 22 (2015) 425–433.

[49] M.C. Ncibi, M. Sillanpää, Optimized removal of antibiotic drugs from aqueous solutions using single, double and multi-walled carbon nanotubes, J. Hazard. Mater. 298 (2015) 102–110.

[50] Z.H. Li, L. Schulz, C. Ackley, N. Fenske, Adsorption of tetracycline on kaolinite with pH-dependent surface charges, J. Colloid Interface Sci. 351 (2010) 254–260.

[51] A. Ungurean, M. Oltean, L. David, N. Leopold, J.P.P. Ramalho, V. Chis, Adsorption of sulfamethoxazole molecule on silver colloids: A joint sers and dft study, J. Mol. Struct. 2014 (1073) 71–76.

[52] I. Braschi, G. Gatti, G. Paul, C.E. Gessa, M. Cossi, L. Marchese, Sulfonamide antibiotics embedded in high silica zeolite y: A combined experimental and theoretical study of host-guest and guest-guest interactions, Langmuir 26 (2010) 9524–9532.